IL NUOVO CIMENTO VOL. 20 D, N. 12 Dicembre 1998

Finite-difference time domain acoustic-wave algorithm

E. IKATA (1) and G. TAY (2)

(1) *Physics Department, College of Education - P.M.B. 5047, Port Harcourt, Nigeria*
(2) *Physics Department, Rivers State University of Science and Technology Nkpolu, Port Harcourt, Nigeria*

(ricevuto il 18 Agosto 1997; revisionato il 10 Giugno 1998; approvato il 24 Giugno 1998)

Summary. — A time domain numerical procedure is presented for a simulation of acoustic-wave phenomena. The technique is an adaptation of the finite-difference time domain (FDTD) approach usually applied to model electromagnetic waves. Simple illustrations of propagation in a nondissipative, infinite, homogeneous medium are provided. In scattering by a soft target the interior fields show that for an acoustically denser target the wave penetrates the target with a magnitude greater than the incident-wave amplitude. Also, the interior acoustic pressure field consists of a pair of high-pressure bands sandwiching a low-pressure band.

PACS 43.35 – Ultrasonic, quantum acoustics, and physical effects of sound.
PACS 02.70.Bf – Finite-difference methods.

1. – Introduction

A leap-frog method [1] for the numerical solution of the hyperbolic partial differential equation has been earlier adapted by Yee [2] to model the behaviour of electromagnetic waves, in which case it is called a finite-difference time domain (FDTD) procedure. This procedure for solving various types of electromagnetic-wave phenomena is currently well developed and quite suited for modelling problems in which the time parameter appears explicitly [3, 4]. What distinguishes a finite-difference time domain technique from other procedures which approximate the partial derivatives using finite differences [5, 6] is that in FDTD a wave equation is first decomposed into two coupled first-order equations before applying the finite-difference approximation. A similar approach has been used by Chow [7] to model the propagation of a sine wavelet in a 1D pipe having one of its ends closed, without the half-index scheme. In this paper the finite-difference time domain technique is adapted to model acoustic-wave phenomena.

An acoustic wave is a common example of a scalar field. It is a small disturbance in pressure and density which propagates in a compressible medium. Since fluids exhibit fewer restraints to deformation, the restoring force responsible for wave propagation is simply due to a pressure change. Using a field approach to describe the state of the

fluid in motion, the relevant field functions are: the density $\varrho(\mathbf{r}, t)$, particle velocity $\mathbf{V}(\mathbf{r}, t)$ and pressure $p(\mathbf{r}, t)$, where $\mathbf{r}$ is a position vector and t is time. We use the word "field" in the ordinary mathematical sense, which implies a function of space (and time), and not in the extended physical sense. Since the disturbance is small, it is possible to replace the equations governing the acoustic wave with their linear equivalents. Consequently, the equation of motion reduces to

$$\varrho_0 \frac{\partial \mathbf{V}}{\partial t} = -\nabla P , \tag{1}$$

where ϱ_0 is a constant equilibrium density of the medium, $P = (p - p_0)$ is an acoustic pressure and p_0 the equilibrium pressure. Similarly, in this limit, the equation of continuity assumes the form

$$\frac{\partial P}{\partial t} = -B \nabla \cdot \mathbf{V} , \tag{2}$$

where B is the adiabatic bulk modulus of the fluid.

Upon differentiating (2) with respect to time and using (1), one easily obtains the wave equation for the acoustic pressure:

$$\nabla^2 P = \frac{1}{v^2} \frac{\partial^2 P}{\partial t^2} ; \qquad v = \sqrt{\frac{B}{p_0}} , \tag{3}$$

where v is the wave propagation speed.

Equations (1) and (2) are those to be discretized in a finite-difference time domain model of acoustic phenomena. Earlier finite-difference approaches to the acoustic-wave problem made use of the wave equation (3) directly [5, 8]. Observe that, because of the linearization implied in (1) and (2), the model is subject to this constraint, *i.e.*, it is suitable so long as the disturbance is small. This is also true for models using (3), though not obvious. The two coupled first-order eqs. (1) and (2) are equivalent, in the rectangular system (x, y, z), to the following system of equations:

$$\begin{cases} \varrho_0 \dfrac{\partial V_x}{\partial t} = -\dfrac{\partial P}{\partial x} , \quad \varrho_0 \dfrac{\partial V_y}{\partial t} = -\dfrac{\partial P}{\partial y} , \quad \varrho_0 \dfrac{\partial V_z}{\partial t} = -\dfrac{\partial P}{\partial z} , \\ \dfrac{\partial P}{\partial t} = -B \left(\dfrac{\partial V_x}{\partial x} + \dfrac{\partial V_y}{\partial y} + \dfrac{\partial V_z}{\partial z} \right). \end{cases} \tag{4}$$

The set of four coupled partial differential equations (4) is the basis for a finite-difference time domain algorithm describing a general acoustic-wave problem. However, assuming that the modelled problem has no variation in the z-direction, then (4) reduces to

$$\begin{cases} \varrho_0 \dfrac{\partial V_x}{\partial t} = -\dfrac{\partial P}{\partial x} , \quad \varrho_0 \dfrac{\partial V_y}{\partial t} = -\dfrac{\partial P}{\partial y} , \\ \dfrac{\partial P}{\partial t} = -B \left(\dfrac{\partial V_x}{\partial x} + \dfrac{\partial V_y}{\partial y} \right), \quad V_z = \text{const} . \end{cases} \tag{5}$$

An FDTD algorithm approximates the continuous-wave field in space by sampled data analogues at distinct points in a finite space-time lattice using finite differences. Consequently, the differential equations are replaced with difference equations and wave phenomena are modelled by repeatedly implementing the difference equations equivalent to the differential equations. This results in a simulation of the actual wave by sampled numerical data analogues "travelling" in a data space stored in a computer.

Simple illustrations using the technique are provided. First, we model the propagation of an acoustic signal in a uniform nondissipative medium. Next, the finite-difference time domain acoustic-wave algorithm is used to simulate the interaction of an acoustic wave with various 2D acoustically soft targets. Our interest concerns the interior field. An accurate determination of the acoustic field within an arbitrary, inhomogeneous, soft target is both an important theoretical problem and a pratical desire, given the increasing use of various types of acoustic signals for diagnosis and therapy in medicine. Exact analytic solutions are possible only for simple targets, which may be solved using, say, separation of variables. For complicated targets like body organs, one must resort to a numerical method if a realistic model is to be examined. An interesting feature of the FDTD technique is its ability to easily handle inhomogeneities through a local specification of medium parameters.

2. – FDTD **acoustic algorithm**

In modelling electromagnetic phenomena, the common FDTD symbolism is that introduced by Yee [2]. Following Yee's notation, a function of space and time is represented as

$$F^n(i, j, k) = F(i\delta x, j\delta y, k\delta z, n\delta t), \tag{6}$$

where i, j, k, n are integers, δx, δy and δz are space increments along the respective axes, and δt is a time increment. The space and time derivatives are replaced with finite-difference expressions which are second-order accurate in the increments *via* a Taylor series expansion:

$$\frac{\partial F(x_0)}{\partial x} = \frac{F(x_0 + (1/2)\,\delta) - F(x_0 - (1/2)\,\delta)}{\delta} + \mathrm{O}(\delta^2), \tag{7}$$

where x_0 is the expansion point and δ is an increment in either time or space.

To achieve the accuracy of (7) and to realize all the space derivatives, the field components about a cell of the lattice are positioned as shown in fig. 1. The field placement scheme of fig. 1a) is slightly different from that introduced by Yee. This is due to the longitudinal nature of acoustic waves. The use of a 2D Yee cell will lead to inappropriate conclusions when the time-stepping relations resulting from (5), or its 3D equivalent, are given a contour integral interpretation [9]. It is a fundamental difference which is apparent on applying finite-difference time domain to acoustic-wave simulation. To achieve the accuracy of (7) for a time derivative, the field functions are evaluated at alternate half-time steps. Adopting the half-index scheme and placing the field functions on a lattice as in fig. 1a) give the system of finite-difference

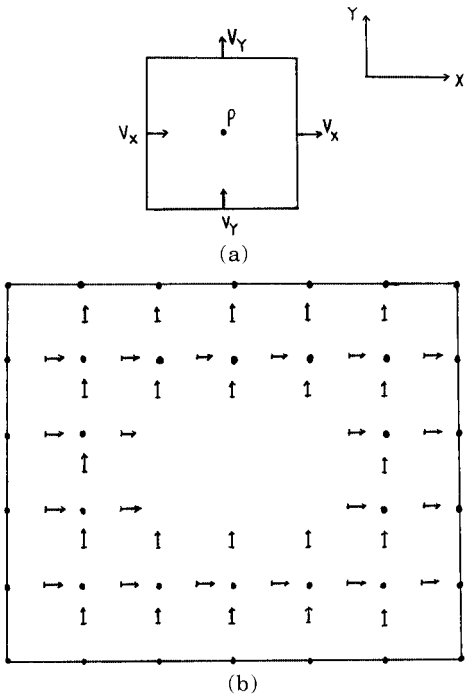

Fig. 1. – a) Acoustic wave field placement scheme. b) 2D computation space and boundary.

time-stepping relations which replace (5), thus

$$
(8)\qquad \begin{cases} V_x^{n+1/2}(i+1/2,\,j) = \\ \qquad = V_x^{n-1/2}(i+1/2,\,j) - \dfrac{\delta t}{\varrho_0(i+1/2,\,j)\,\delta x}\,[P^n(i+1,\,j) - P^n(i,\,j)], \\ V_y^{n+1/2}(i,\,j+1/2) = \\ \qquad = V_y^{n-1/2}(i,\,j+1/2) - \dfrac{\delta t}{\varrho_0(i,\,j+1/2)\,\delta y}\,[P^n(i,\,j+1) - P^n(i,\,j)], \\ P^{n+1}(i,\,j) = P^n(i,\,j) - \dfrac{B(i,\,j)\,\delta t}{\delta x}\,[V_x^{n+1/2}(i+1/2,\,j) - V_x^{n+1/2}(i-1/2,\,j)] - \\ \qquad - \dfrac{B(i,\,j)\,\delta t}{\delta y}\,[V_y^{n+1/2}(i,\,j+1/2) - V_y^{n+1/2}(i,\,j-1/2)]. \end{cases}
$$

The choice of space and time increments is motivated by reasons of accuracy and stability, respectively. In electromagnetic models a space increment of about a tenth of the minimum wavelength gives acceptable results. To ensure the stability of the time-

stepping algorithm, the time increment should satisfy the Courant criterion [10]

$$v_{\max}\,\delta t \leqslant \left(\frac{1}{\delta x^2}+\frac{1}{\delta y^2}\right)^{-1/2}, \tag{9}$$

where $v_{\max}$ is the maximum wave speed in a problem.

The time stepping relations (8) are for updating the field function at an interior grid point. In a numerical experiment, the size of a computation space is limited using a lattice truncation scheme [11]. Here use is made of the 2D computation lattice and boundary of fig. 1b). Observe from fig. 1b) that the velocity field function occurring along the computation boundary can be determined using the interior region time-stepping relations (8). However, to calculate the pressure field function along a computation boundary, using (8), requires field values outside the specified domain—this is what necessitates the use of a lattice truncation scheme.

Details on implementing a lattice truncation scheme depend on the kind of problem modelled. In ordinary wave propagation there are two approaches depending on whether: *a*) the domain includes a source of radiation, or *b*) the field enters the domain from sources located outside. In the first case, the lattice truncation scheme involves implementing a radiation boundary condition about the entire boundary surface (or contour) defining the space. However, in the other situation, the lattice truncation scheme involves implementing a radiation boundary condition along only those planes (or lines) normal to the propagation direction while a plane-wave condition is implemented along the remaining planes (or lines) parallel to the propagation direction. Consequently, the lattice truncation scheme used here includes

a) a plane-wave (Neumann-type) condition,

b) a first-order Bayliss-Turkel radiation boundary condition [12], and

c) a second-order Bayliss-Turkel radiation boundary condition.

These are discretized *via* the Mur differencing scheme [13]. Thus the time-stepping relations for our lattice truncation scheme are

$$P^{n+1}(i,0)=P^{n+1}(i,1), \tag{10a}$$

$$P^{n+1}(i,NY)=P^{n+1}(i,NY-1), \tag{10b}$$

$$P^{n+1}(0,j)=P^{n}(1,j)+\left(\frac{1-\gamma}{1+\gamma}\right)[P^{n}(0,j)-P^{n+1}(1,j)], \tag{10c}$$

$$P^{n+1}(NX,j)=P^{n}(NX-1,j)+\left(\frac{1-\gamma}{1+\gamma}\right)[P^{n}(NX,j)-P^{n+1}(NX-1,j)], \tag{10d}$$

$$\begin{aligned}P^{n+1}(0,j)=&-P^{n-1}(1,j)-\frac{1-\gamma}{1+\gamma}[P^{n+1}(1,j)+P^{n-1}(0,j)]+\\&+\frac{2}{1+\gamma}[P^{n}(0,j)+P^{n}(1,j)]+\frac{\gamma^2}{2(1+\gamma)}\cdot\\&\cdot[P^{n}(0,j+1)-2P^{n}(0,j)+P^{n}(0,j-1)+P^{n}(1,j+1)-2P^{n}(1,j)+P^{n}(1,j-1)],\end{aligned} \tag{10e}$$

where $\gamma = v\,\delta t/\delta x$.

Equations (10*a*)-(10*b*), (10*c*)-(10*d*) and (10*e*) are the discretized equivalents of a plane-wave condition, a first-order, and a second-order Bayliss-Turkel radiation boundary condition [12], respectively. The set of lattice truncation scheme time-stepping relations (10*a*)-(10*d*) coupled to the interior-region time-stepping relations (8) provides a complete set of time-stepping relations for the FDTD acoustic algorithm. However, eqs. (10*c*), (10*d*) are appropriate in the absence of a target. In a scattering problem eqs. (10*c*), (10*d*) should be replaced with the equivalent expressions for a second-order Bayliss-Turkel condition (10*e*) for acceptable results. This is what has been done in subsect. 3·2.

Finally, a plane-wave source is simulated by making any plane in the computation space "radiate" into the domain. Experiments show that an easier simulation results when this "radiating" plane coincides with a computation boundary plane in the case of time-harmonic plane waves. Also, transient plane waves may be simulated either *via* a "radiating" boundary plane or by directly placing a pulse within the computation domain. However, because of smoothness requirements, it is usual to use a plane Gaussian pulse [14]:

$$g(t) = A \exp\left[-\left(\frac{4(t - t_0)}{T} \right)^2 \right], \tag{11}$$

where T is the pulse width and t_0 is the time lapse before the pulse enters the domain.

3. – Numerical results

3·1. *Wave tracking in a uniform medium.* – Our numerical experiment models the propagation of an acoustic wave in sea water, which is assumed to be an infinite homogeneous medium. We take the fluid density and bulk modulus to be $998\ \mathrm{kg\,m^{-3}}$ and $2.18 \times 10^9\ \mathrm{N\,m^{-2}}$, respectively. We consider three cases. In the first case (fig. 2), we imagine a "bang" to be released at some point within the fluid, while in the second case (fig. 3), we assume that a transient plane wave enters the medium from infinity. Finally, in the third case (fig. 4), we imagine that a time-harmonic plane wave enters the medium from infinity. The horizontal arrows in the figures indicate the direction of propagation. The pressure magnitude is in arbitrary units. In all situations, our concern is limited to the free propagation of the wave in the absence of inhomogeneities.

From fig. 2a), we observe how the wave propagates uniformly in all directions after release. (Here, this is represented as "left"- and "right"-propagating waves.) After some time, the main pulses leave the computation space and what remains is a trailing alternating signal (fig. 2d)) termed "ringing" in the literature. When a Gaussian pulse is used as the source of a transient plane wave (fig. 3) the "ringing" observed in fig. 2 is almost absent (compare fig. 2b) with 3b)). Consequently, the ringing effect is attributed to the abrupt nature of the half-sine pulse used to model the "bang". The pulse of fig. 3d) is propagating to the left and is a result of the imperfect radiation boundary condition used to model infinite space at the computation boundary. However, given its amplitude, this reflection is only about 18 per cent. The Gaussian pulse width is taken to be $0.203\ \mu\mathrm{s}$ and the pulse is assumed to enter the domain after 10 time steps.

Figure 4 is representative of a numerical model for time-harmonic plane-wave propagation. The influence of the source location is examined, for the cases when the source is implemented along a computation boundary and within the computation

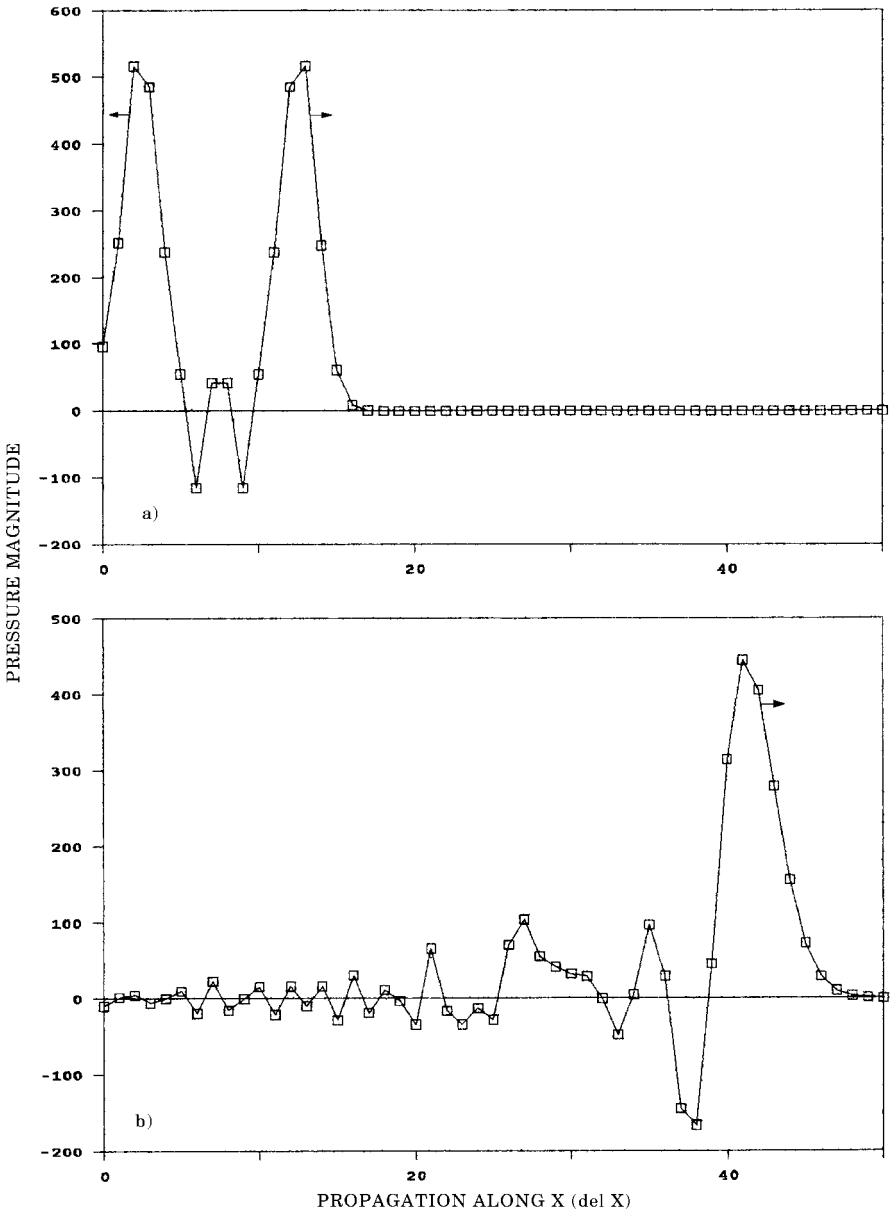

Fig. 2. – a) Pulse after 10 time steps. b) Pulse after 70 time steps.

space. Though the wave amplitude is held constant, one finds the ambient field to be a function of the source placement scheme (fig. 4c)). When the plane-wave source is implemented along an interior lattice plane ($I = 2$) the ambient field which results in the neighbourhood of such points is slightly different compared to when the source is implemented along a computation boundary plane ($I = 0$), fig. 4b). Thus, implementing a harmonic plane-wave source along a lattice boundary leads to an easier simulation of

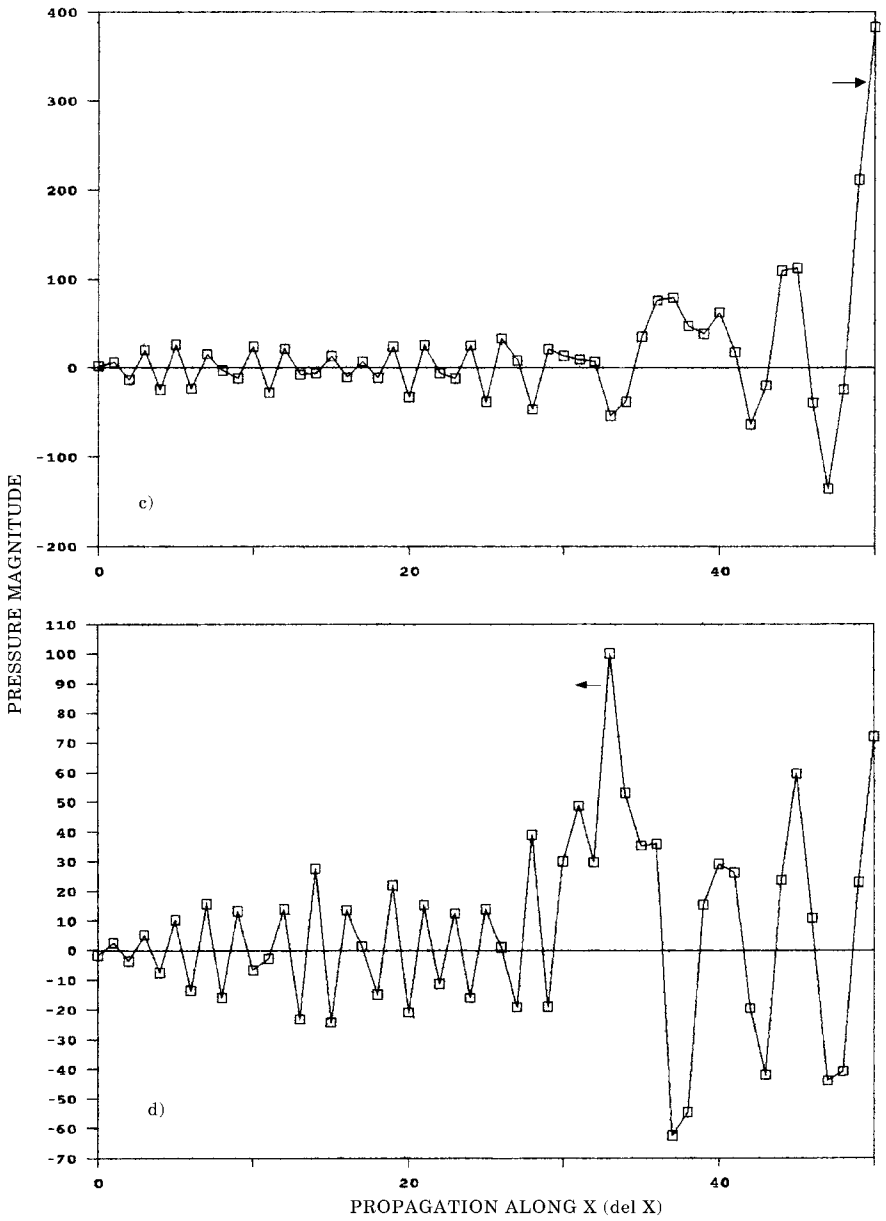

Fig. 2. – (*Continued*.) c) Pulse after 90 time steps. d) Pulse after 150 time steps.

the physical situation and to follow the recommendation of Taflove and Brodwin [3] in this respect does require caution. Caution is particularly necessary when the plane-wave source is implemented along an interior lattice plane (say, at $I = 2$) in a code for scattering by a soft target. In this case, without variable time stepping, the Courant criterion often imposes on us a very small time increment. Consequently, for a

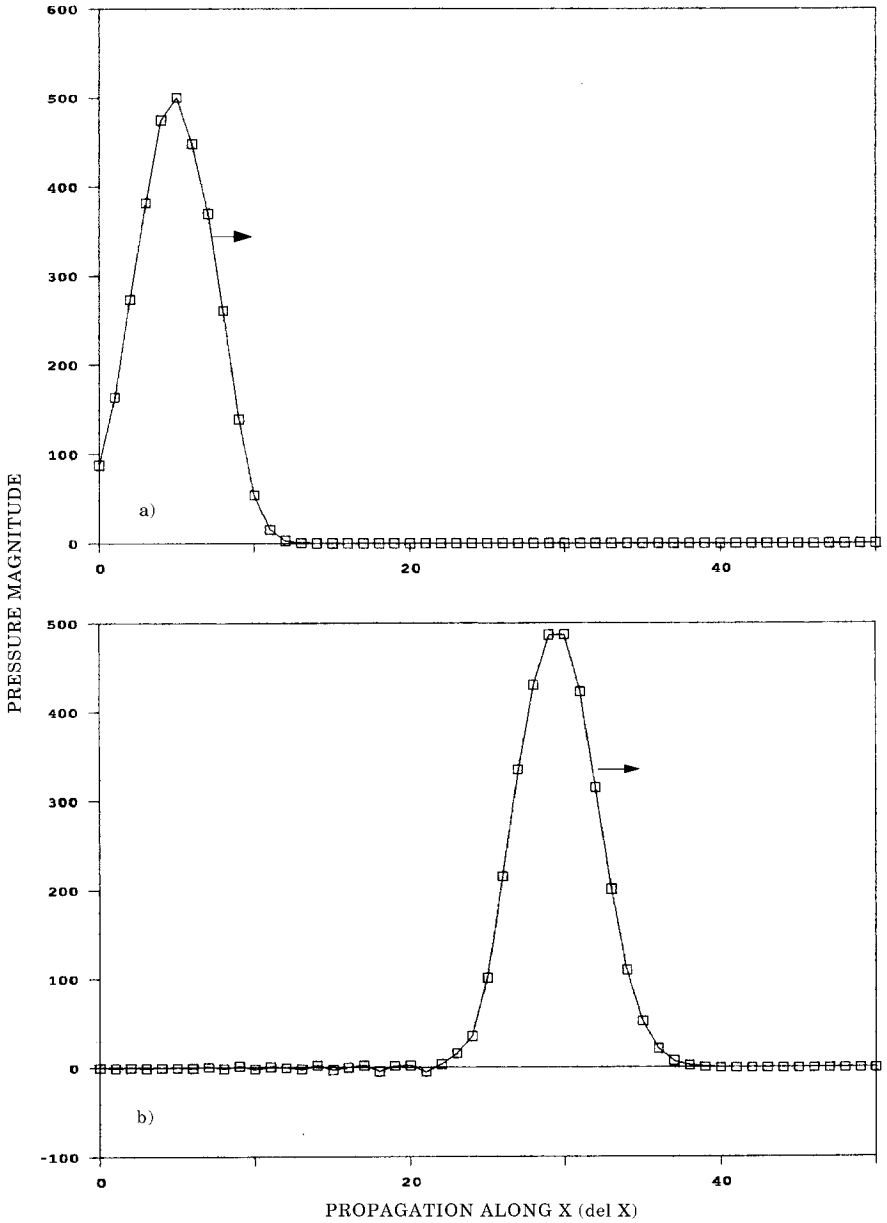

Fig. 3. – a) Gaussian pulse after 20 time steps. b) Gaussian pulse after 70 time steps.

numerical plane-wave source of given amplitude, the ambient field amplitude within the computation space is twice the physical value when one implements the plane-wave source along an interior lattice plane (fig. 4c)). Thus, though the plane-wave source condition of Taflove and Brodwin [3] allows one to implement a radiation boundary condition over all the computation boundary, to absorb out-going scattered waves, field

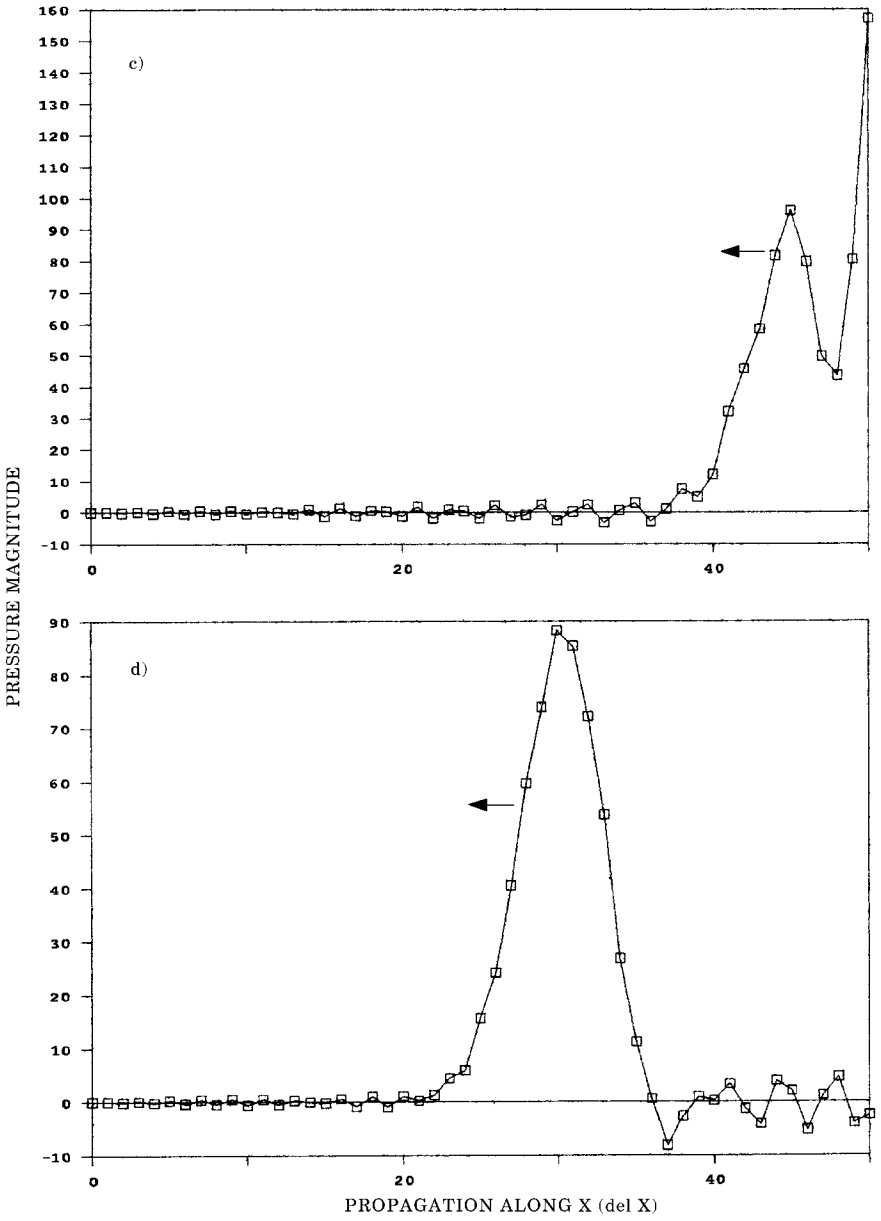

Fig. 3. – (*Continued*.) c) Gaussian pulse after 120 time steps. d) Gaussian pulse after 150 time steps.

values calculated using this source placement scheme will often be twice that due to a physical source. We notice, also, from fig. 4a) that until the wave completely fills the computation space the amplitude, especially of the leading part, is less than the coded amplitude for the source. For these experiments the Courant factor is taken as 0.7 which is close enough to the theoretical limit, 0.707, in 2D. Studies suggest that in order

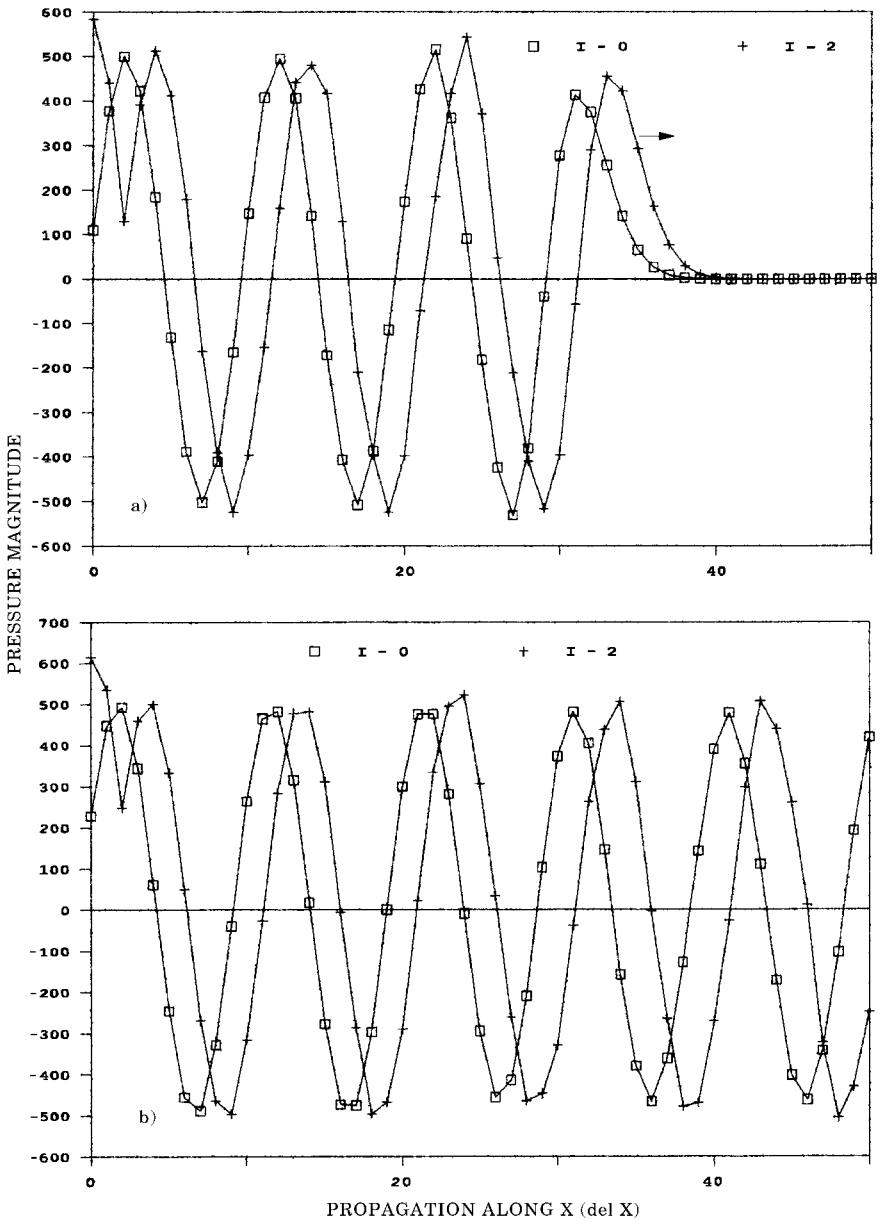

Fig. 4. – a) Wave after 70 time steps. b) Wave after 150 time steps.

to reduce numerical noise in FDTD, one should use a Courant factor very near the theoretical limit [15].

3·2. *Interior acoustic field in a soft target.* – Numerical experiments which describe the scattering of an acoustic signal by a soft target are presented next. These experiments provide the (near-) fields in the immediate neighbourhood of a target at

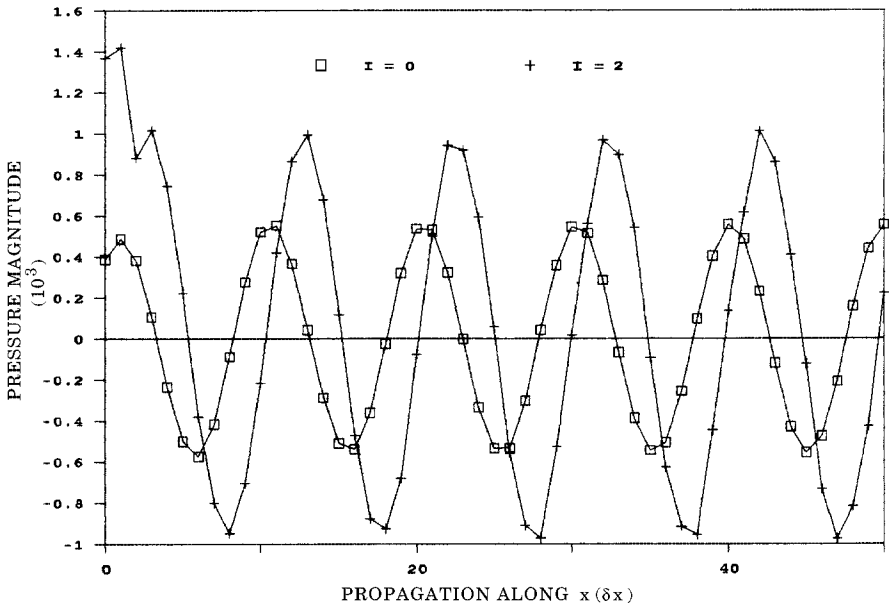

Fig. 4. – (*Continued*.) c) Ambient field in computation space.

various times. To partially compensate for numerical noise, our FDTD codes calculate a scattered field by subtracting an FDTD (instead of a physical) incident field from the computed total field. The computation of a scattered field in an FDTD open-region scattering code is not optional (even when the knowledge of the total field is what one requires) since, in principle, the radiation boundary condition implemented at a lattice truncation plane is only applicable to outgoing waves. Our concern is with the interior field. The angle of incidence in all cases is zero degrees. For an incident time-harmonic plane wave, the target characteristic size ka is about 1.5, where k is the exterior region propagation constant and a is one-half the longitudinal dimension of a target. In all situations, the target is positioned approximately within the center of our computation space. The computation space is a 50×50 cell lattice and a radiation boundary condition (10*e*), instead of (10*c*), (10*d*), is implemented at between 10 and 15 space increments from a target surface, depending on the target geometry. The target shapes are a square, a circle and an ellipse. The numerical problem simulates a piece of quartz in sea water, with the incident wave originating in the water. The medium parameters for quartz are $2650\ \mathrm{kg\,m^{-3}}$ and $3.3 \times 10^{10}\ \mathrm{N\,m^{-2}}$, respectively, for the density and bulk modulus. The target dimensions are: square side 0.6 m; circle radius 0.3 m; ellipse semi-axes $\{0.3, 0.2\ \mathrm{m}\}$. The acoustic wave is assumed to have a wavelength of 0.2 m in sea water. The space increment is taken as 0.02 m and, consequently, the time increment which satisfies the Courant criterion within the target is 14.026 μs. This implies a Courant factor of about 0.293.

The computed results after 500 time steps are sampled for the absolute value of the acoustic pressure $P(i, 25)$ and $P(i, 15)$ along $J = 25$ and 15, respectively. These are represented graphically for the various targets. Figure 5 is for a square target, fig. 6 is for a circle and fig. 7 is for an ellipse. In all these figures, along the line $J = 25$, the

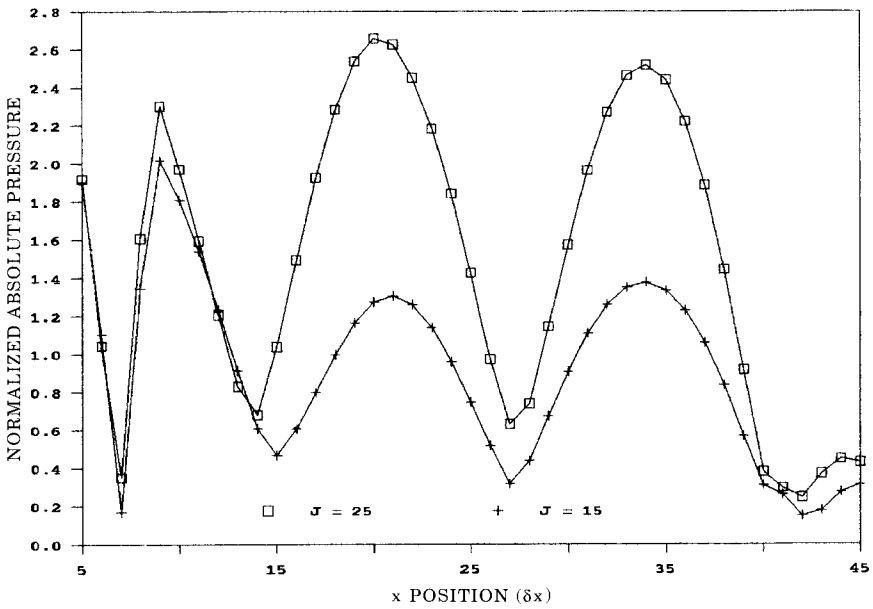

Fig. 5. – Interior pressure field in square target.

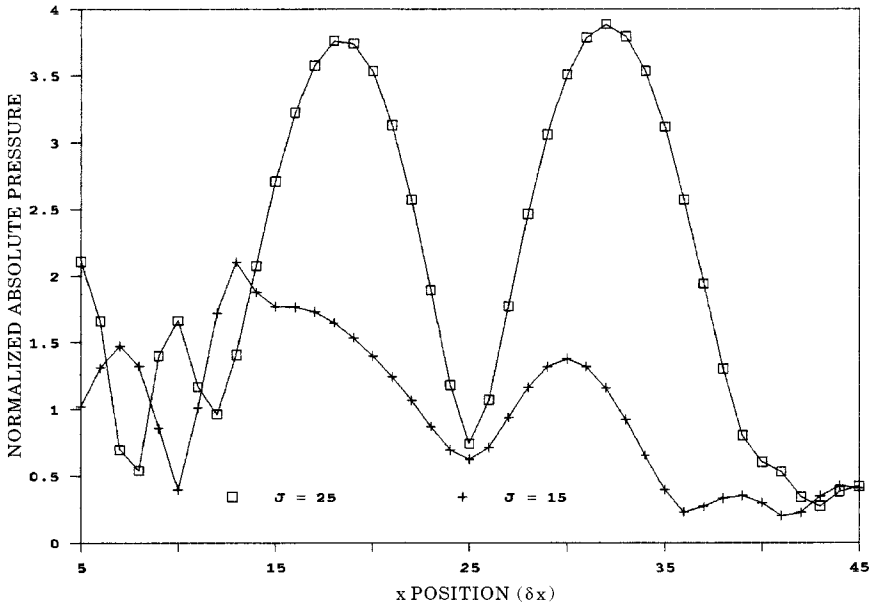

Fig. 6. – Interior pressure field in circular target.

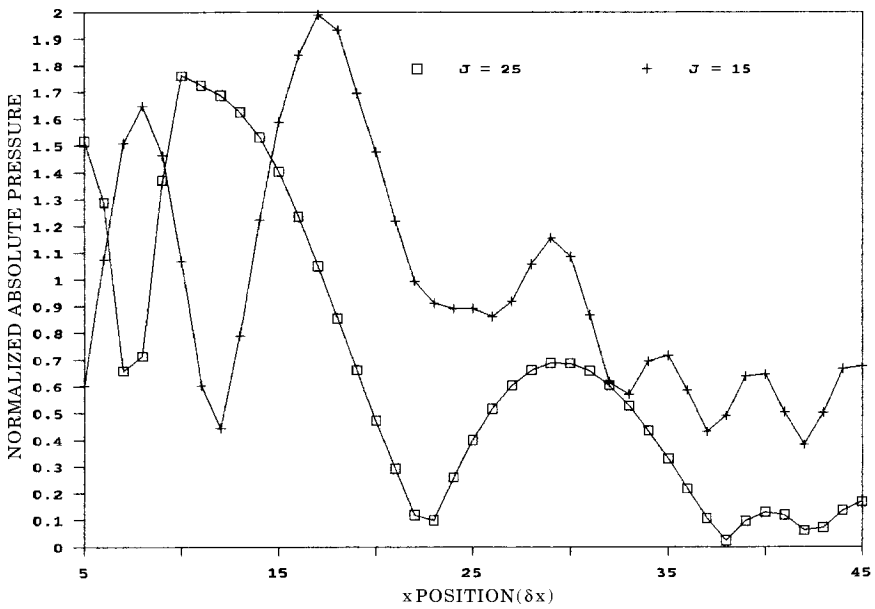

Fig. 7. – Interior pressure field in elliptical target.

target occupies the interval $10 \leqslant i \leqslant 40$. From these plots we observe that the wave penetrates the target with a magnitude greater than the incident-wave amplitude. This may be attributed to the target being acoustically denser than the exterior region. Furthermore, as is clearly evident from figs. 5 and 6, the interior pressure field consists mainly of two bands of high pressure sandwiching a low-pressure band, along the middle of the target. These high-pressure bands have a magnitude usually greater than one-and-a-half times the incident-wave amplitude. Thus, compressional stresses do result within the target that may cause it to be crushed. Finally, the magnitude of the interior acoustic pressure attainable is highest in a circular target. The reason for this is not obvious.

4. – Conclusion

The numerical technique has been shown to be suitable for modelling the propagation of acoustic waves in a nondissipative, infinite, homogeneous medium. Effects such as uniform spreading and distribution of wave energy in all directions, as in the case of a "bang", are clearly illustrated. Also, the use of FDTD to model acoustic-wave interaction with soft targets is illustrated. For the examined problem one finds that, basically, an acoustic wave penetrates a denser target with increased magnitude. It is likely that the normalized interior acoustic pressure may not be up to, say, 3.8 as is evident from fig. 6, because it was earlier shown that using a very low Courant factor, as we were constrained to do, does lead to a relatively high nonphysical ambient field. However, the qualitative feature of the interior acoustic pressure attaining a normalized absolute value greater than unity is physical and, if one compensates for the low Courant factor, a value of about 2.0 is more likely. The

presence of the high- and low-pressure bands may be attributed to an interference effect. Thus, when an acoustically denser soft target is illuminated by a time-harmonic plane acoustic wave, compressional stresses are more likely to be induced within the target.

* * *

We acknowledge helpful discussions held with Dr. I. MBELEDOGU of the Department of Mathematics and Computer Science, University of Port Harcourt, Port Harcourt, and appreciate the good will of the management at the College of Education, Port Harcourt, who provided computing facilities for this work.

REFERENCES

[1] LAPIDUS L. and PINDER G. F., *Numerical Solution of Partial Differential Equations in Science and Engineering* (Wiley, New York) 1982.
[2] YEE K. S., *IEEE Trans. Antennas Propagat.*, **AP-13** (1966) 302.
[3] TAFLOVE A. and BRODWIN M. E., *IEEE Trans. Microw. Theory Tech.*, **MTT-23** (1975) 623.
[4] TAFLOVE A. and UMASHANKAR K. R., in *Progress in Electromagnetic Research*, Vol. **2**, edited by M. A. MORGAN (Elsevier, Amsterdam) 1989, p. 287.
[5] ENGQUIST B. and MAJDA A., *Math. Comput.*, **31** (1977) 629.
[6] KRIEGSMANN G. A. and MORAWETZ C. S., *SIAM J. Sci. Stat. Comput.*, **1** (1980) 371.
[7] CHOW C. Y., *An Introduction to Computational Fluid Mechanics* (Seminola Publ., Boulder) 1983, p. 192.
[8] KRIEGSMANN G. A. and SCANDRETT C. L., *J. Acoust. Soc. Am.*, **79** (1986) 9.
[9] TAFLOVE A., UMASHANKAR K. R., BEKER B., HARFOUSH F. and YEE K. S., *IEEE Trans. Antennas Propagat.*, **AP-36** (1988) 247.
[10] COURANT R., FRIEDRICHS K. and LEWY H., *Math. Ann.*, **100** (1928) 32.
[11] MORGAN M. A., in *Progress in Electromagnetic Research*, Vol. **2**, edited by M. A. MORGAN (Elsevier, Amsterdam) 1989, p. 1.
[12] BAYLISS A. and TURKEL E., *Commun. Pure Appl. Math.*, **33** (1980) 707.
[13] MUR G., *IEEE Trans. Electromag. Compat.*, **EMC-23** (1981) 377.
[14] CANGELLARIS A. C. and MEI K. K., in *Progress in Electromagnetic Research*, Vol. **2**, edited by M. A. MORGAN (Elsevier, Amsterdam) 1989, p. 249.
[15] CANGELLARIS A. C., *Differential Equations Based Methods for Electromagnetic Wave Scattering and Radiation: Review of State of the Art and Future Direction, 23rd URSI General Assembly, Prague, 1990.*